Identification and Quantitation of Bone Marrow Adipocytes by Immunostaining

Yimeng Chen

Master´s thesis

Åbo Akademi University
Department of Biosciences
Faculty of Science and Engineering
26.5.2022

Master´s degree in Biomedical Imaging
Specialization field: Cell Biology

Credits: 4 0 ECTS

Supervisors:

1: Kaisa Ivaska

2: Nicko Widjaja

Passed:

Grade:

Abstract

ÅBO AKADEMI UNIVERSITY

Department of biosciences
Faculty of science and engineering

Yimeng Chen: Identification and Quantitation of Bone Marrow Adipocytes by Immunostaining

Master´s thesis, 48 pp., 1 Appendix

Specialization level: cell biology
5 2022

Bone marrow adipocytes (BMAds) have been found to impact other cell populations inside the marrow and they can influence the entire body, but the role of adipocytes in bone physiology has been poorly understood. BMAds can be identified in histological samples. They are commonly identified as unstained white and round objects in sections when using the hematoxylin and eosin (H&E) staining method. There is a need for additional specific detection by immunohistochemistry (IHC) to discern microvasculature from adipocytes. The aim of the study was to develop and optimize a method for the identification and quantitation of BMAds in formalin-fixed paraffin-embedded (FFPE) long bone tissue sections by immunostaining of adipocyte-specific protein perilipin-1. Secondly, our aim was to apply the IHC method and a semi-automated ImageJ script to identify and quantitate BMAds in rat long bone sections under two experimental conditions. The staining protocol was optimized at the beginning. Various staining parameters were optimized to immunobiologically stain rat perilipin-1 in FFPE long bone sections. After that, a workflow of image analysis was developed. Quantitative analysis was carried out by using segmentation-based approaches utilizing common bioimage analysis software. μCT was used to obtain volumetric bone mineral density (BMD) and structural parameters on bone quantity and phenotype. Tibiae were collected from rats supplemented with high-fat diet and control rats to test and verify the optimized protocol. The final optimized protocol was established from all parameters (deparaffinization, antigen retrieval, permeabilization, blocking, antibody concentration and autofluorescence reduction). The optimized semi-automated quantitation method was comparable to the manual counting. (R=0.959)
The number of BMAds was typically 300-500 /mm^2 in the bone marrow region and the size range of cells was about 700 to 1000 μm^2. Our optimized IHC method brings improvement over H&E as it can positively stain BMAds. It can be applied to histological bone tissue sections. An improved quantitation analysis based on this IHC method was presented by the end. Pilot studies from the μCT from different groups showed that with the high-fat diet, there were some decreases in percent bone volume, bone surface, and trabecular number. A reduction in the total porosity can be seen in the exercise group. There was a slight increase in BMD with high-fat intervention in both trabecular and cortical bones. The method should be suitable to be applied to samples collected from *in vivo* experiments.

Keywords: bone, bone marrow adipocyte, immunostaining, immunohistochemistry

LIST OF USED ABBREVIATIONS

AF	Autofluorescence
BM	Bone marrow
BMA	Bone marrow adiposity
BMAd	Bone marrow adipocyte
BMAT	Bone marrow adipose tissue
BMD	bone mineral density
DEXA	Dual-energy X-ray absorptiometry
EDTA	Ethylenediaminetetraacetic acid
EIER	Enzyme-Induced Epitope Retrieval
EtOH	Ethanol
FA	Formic acid
FFPE	Formalin-Fixed Paraffin-Embedded
H&E	Hematoxylin and Eosin
HFD	High-fat-diet
HF-EX	High-fat-diet and exercise
HIER	Heat-induced epitope retrieval
IHC	Immunohistochemistry
MAT	Marrow adipose tissue
MRI	Magnetic resonance imaging
PBS	Phosphate-buffered saline
PLIN1	Perilipin-1
QCT	Quantitative computed tomography
R	Correlation coefficient
RT	Room temperature
RTER	Room Temperature Epitope Retrieval
SBB	Sudan Black B
SC	Sodium citrate
SD	Sprague Dawley
TBS	Tris-buffered saline
TBST	Tris Buffered Saline with Tween® 20
Tif	Tagged Image File Format
µCT	Micro-computed tomography

1. REVIEW OF THE BACKGROUND AND LITERATURE

1.1. Bone and Bone marrow adipocytes (BMAds)

Bone tissue is a type of specialized connective hard tissue with a honeycomb-like network of trabeculae at the inner matrix, and in the compact bone, the matrix is tightly packed, which helps to give the bone rigidity. The major types of bone cells are osteogenic progenitor cells, bone-forming osteoblasts, osteocytes, and bone-resorbing osteoclasts (see Figure 1 A). Other tissues and structures found in bones include bone marrow, bone lining endosteum and periosteum, nerves, blood vessels and cartilage (Florencio-Silva et al., 2015). At the macrostructure level, bone is separated into the compact (or cortical) and spongy (or trabecular) types. In cross-section, the end of a long bone such as the femur (see Figure 1 B) has a dense cortical shell with a porous, cancellous interior (Betts et al., 2013).

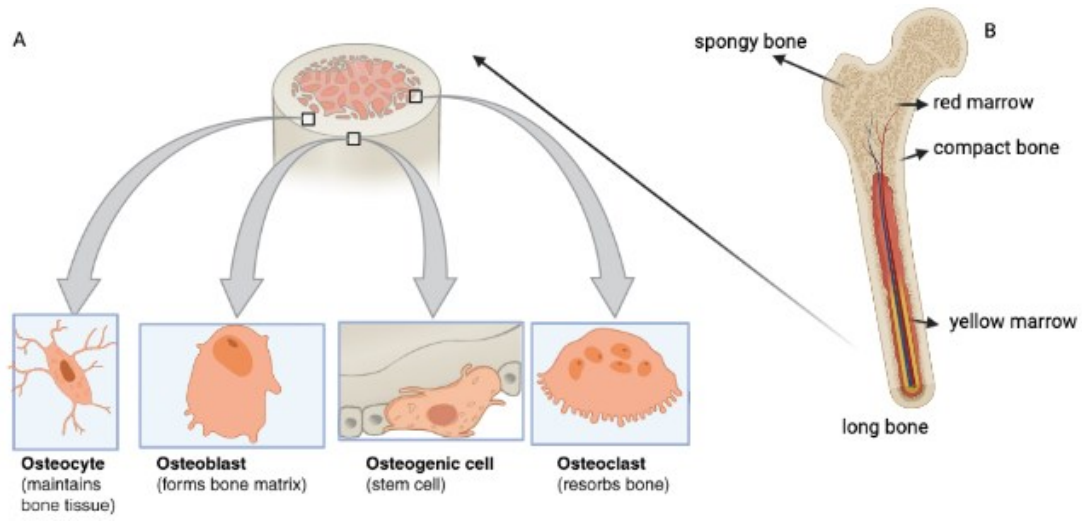

Figure 1. A) Four different main types of bone cells. B) The macroscopic structure of a long bone. Figure modified from (Betts et al., 2013).

Bone marrow (BM) contains stem cells for blood cells but also fat cells, the adipocytes. Bone marrow adipose tissue (BMAT) is the collection of adipocytes found within medullary cavities of the skeleton that comprises up to 30% of total fat mass in healthy humans (Scheller et al., 2016). Adipocytes differentiate from the same mesenchymal stromal progenitor cells as the bone-forming osteoblasts (Tencerova and Kassem, 2016). For a long time, bone marrow adipocytes (BMAds) have been considered an inert filler of the marrow cavity and the role of adipocytes

in bone physiology has been poorly understood. BMAT increases with age and in response to certain pathological conditions, such as obesity, anorexia, and bone fragility (Patel et al., 2018; Nouh and Eid, 2015; Johnson and Rabinovitch, 2012; Piotrowska and Tarnowski, 2021).

BMAds have been found to impact other cell populations inside the marrow and they can influence the entire body by the secretion of a characterized set of adipokines, chemokines, hormone-like factors, and other mediators. For example, adipokines affect appetite and satiety, glucose and lipid metabolism, blood pressure regulation, inflammation, and immune functions. They work as a network to regulate inflammation, insulin action, and glucose metabolism locally and systemically. This networking system is changed in obesity (Balistreri et al., 2010).

Ongoing exploration based on gene expression profiles suggests that marrow adipocytes may be different from white adipocytes and brown and beige adipocytes, demonstrating that the BM is a unique fat depot/tissue, distinct from regular white adipocytes (Horowitz et al., 2017; Pham et al., 2020; Attané et al., 2020).

The originally proposed function for BMAds was to secrete adipokines and release unsaturated fatty acids that may act in a paracrine and endocrine way and support energy for other cells in the marrow (Styner et al., 2017). Adiponectin is the most studied adipokine secreted by MAT, particularly in animal models. Adiponectin is mainly secreted by fat cells, and it manages e.g. insulin affectability and energy expenditure. Overweight individuals have a lower convergence of adiponectin; however, it will increment when energy is deficient (Herrmann, 2019).

Rodent studies show an increased amount of marrow fat in diabetic animals (Kim and Schafer, 2016a; Piotrowska and Tarnowski, 2021). There might be a particular marrow lipid immersion profile in diabetes(Kim and Schafer, 2016b). More prominent MAT is related to reduced bone mineral density and MAT might be an arbiter of skeletal fragility in diabetes(Kim and Schafer, 2016b). Circulating lipids, growth hormone alterations, visceral adiposity, and hyperleptinemia have all been related to more prominent marrow fat and may address possible components for the putative impacts of diabetes on marrow fat, albeit different factors probably contribute (Kim and Schafer, 2016a). However, more studies are required to better understand the role of marrow fat in diabetic skeletal fragility as the relationship between adipocytes and bone

is complex: adiposity has associations with bone that are dependent on age, gender, menopausal status, adipose depot, and bone compartment (Kim and Schafer, 2016a).

1.2. Histological stains

Staining is used to highlight important structures of the tissue as well as to enhance tissue contrast for histological study. Histological sectioning and histomorphometry remain the gold standard for the *ex vivo* evaluation and characterization of biological tissues in general, and the evaluation of BMAT, by measurement of adipocyte cell size and cell number (Tratwal et al., 2020a).

1.2.1. Haematoxylin and eosin (H&E)

One of the most common and important histological staining procedures is haematoxylin and eosin (H&E). The H&E stain provides a comprehensive image of the microanatomy of tissues. Haematoxylin precisely stains nuclear components, which include heterochromatin and nucleoli, while eosin-stained cytoplasmic components included collagen and elastic fibres, muscle fibres and red blood cells(Feldman and Wolfe, 2014). Haematoxylin itself is anionic and does not have much affinity to DNA (Renshaw, 2013). Eosin is a type of fluorescent red dye, and it is the most suitable stain for combining with alum haematoxylin to display the general histological structure of the tissue (Bancroft and Layton, 2013). Although eosin is not generally regarded as a fluorescent dye, this dye has been described to have high fluorescence emission.

Today, all tissue specimens are often routinely treated with H&E for histopathological process study. Even though the method is fast, cheap, and tuneable, the H&E mostly provides information about overall structure and morphology; thus, other stains are usually needed. (Alturkistani et al., 2015).

Haematoxylin is arguably the most popular background stain in immunohistochemistry (IHC). When antibodies are used to detect specific proteins through IHC, background stains, such as haematoxylin, are used to simultaneously visualize the cells and the location of a protein of interest. (Onul et al., 2012).

1.2.2. Immunohistochemistry (IHC)

To highlight the important structures of tissue for morphology visualization, various staining techniques can be used. In addition to general histological staining methods, such as using H&E, immunostaining could be applied when studying specific cells and tissues as well. (Fischer et al., 2008)

Immunostaining for tissue uses antibodies to identify the presence of proteins and other antigens in tissue slices (Maity et al., 2013). Either chromogenic detection with a coloured enzyme substrate or fluorescence detection with a fluorescent dye can be used to locate antibody-antigen interactions. It provides essential information about protein localization in intact tissue. IHC can identify products and provide information about where they are located within cells or in the extracellular matrix. This is especially true in the case of bone tissue, which has a variety of cell types and matrix components, each with its own set of protein expression patterns (Idleburg et al., 2015). The advantage of the method is that it can show the spatial localization of various structures formed by cells in tissue (Schaffer and Willerth, 2017).

Two strategies are used for the IHC detection of antigens in tissue: the direct and indirect methods.

The direct IHC-detection method (Figure 2 A) is a one-step detection that involves a labelled antibody reacting directly with the antigen in tissue sections. It utilizes only one antibody, and the procedure is therefore simple and rapid. However, it may suffer from problems with sensitivity due to little signal amplification. Therefore, it is less common than the indirect method. With the direct method, it would be necessary to make custom-labelled antibodies against every antigen of interest.

The indirect IHC-detection method (Figure 2 B) involves an unlabelled primary antibody that reacts with tissue antigen and a labelled secondary antibody that reacts with the primary antibody. The secondary antibody must be targeted against the immunoglobulin G (IgG) of the animal species in which the primary antibody has been produced. This method shows greater sensitivity due to signal amplification through several secondary antibody reactions with different antigenic sites on the primary antibody. But if the target itself was abundantly expressed, e.g., cross-reaction and unspecific binding, there would be a higher risk to detect other unwanted subjects

Aside from that, it also has the advantage that only a relatively small number of standard conjugated secondary antibodies need to be generated. Only one good anti-mouse, anti-rabbit, anti-goat etc, is needed, which detects the constant region of immunoglobulins synthesized in mouse, rabbit, goat etc. The secondary antibody can be labelled with a fluorophore or an enzyme (Buchwalow and Böcker, 2010).

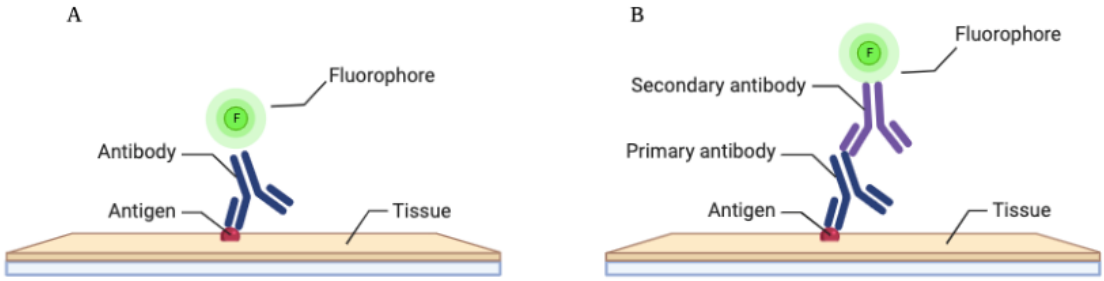

Figure 2. A) The direct IHC-detection method and B) the indirect IHC-detection method. Figure adjusted from (Buchwalow and Böcker, 2010).

1.3. Evaluating BMAds in histological sections

Currently, BMAds are commonly identified by counting the adipocytes as unstained white and round objects (Figure 3) in sections stained with the H&E method. However, there are challenges in these detections, such as the distinction of adipocytes from small blood vessels, which also appear similar to unstained round structures in H&E staining. Additional specific detection by IHC to discern microvasculature from adipocyte ghosts is, thus, highly recommended as a validation step (Tratwal et al., 2020a).

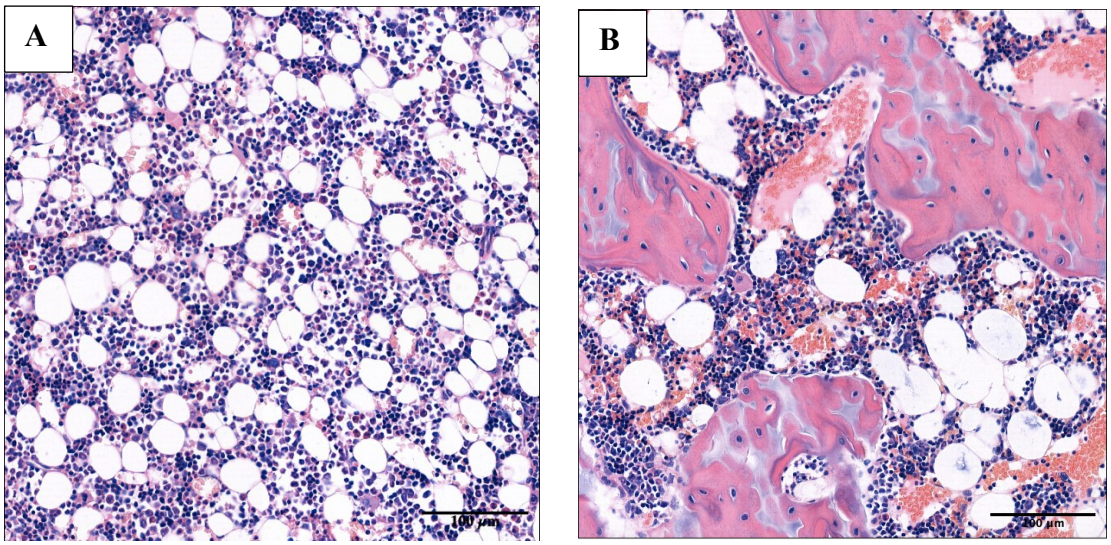

Figure 3. A) H&E stain of BM region at diaphysis and B) at metaphysis (rat tibia, 20x). Pinkish areas are bone trabeculae and white, round objects are bone marrow adipocytes, which contain one large lipid droplet (unstained in H&E).

IHC has not been widely involved in the BMAd studies and that is the reason we would like to implicate IHC for localizing BMAds in the bone tissue samples. BMAds are not grouped in lobules as in most other fat depots, but they are often scattered within the hematopoietic tissue. X-ray QCT has been used already for BMAd studies in animals (Adams, 2009) but its geometrical resolution of it is weak and a preferential loss of photons with low energy leads to under-estimation of the quantity of adipose in long bones (Hardouin et al., 2014).

IHC was used in histology to detect the presence of specific protein markers. It has evolved to complement the H&E and special stain techniques that typically show tissue morphology.

1.4. Perilipin is a marker of adipocytes

Lipid droplets exist in the cytoplasm of almost all types of cells in mammalian tissues, and they play an important role in cellular lipid homeostasis. The neutral lipid core of lipid droplets is covered by a monolayer of phospholipids and cholesterol, and proteins are embedded in it. Proteomics research has revealed more than 200 protein components of lipid droplets, some of which are located only in lipid droplets, while others are also present in other subcellular compartments. Perilipins are one of the most abundant lipid droplet proteins (Zhang et al., 2020).

Adipose cells produce and secrete various physiologically significant proteins, and perilipin is one of the significant proteins produced by adipose cells. Adipocytes can be visualized by utilizing perilipin as a target for IHC (Maity et al., 2013). Perilipin is an intracellular neutral lipid droplet protein that is hormonally managed (Greenberg et al., 1991). This protein is localized exclusively to the surface of intracellular lipid droplets. Perilipin expression is restricted to adipocytes and steroidogenic cells.

Five perilipin genes encode five major perilipin proteins from 1 to 5. Perilipins control lipolysis of stored neutral lipids by cytosolic lipases Perilipin-1(PLIN1) controls lipolysis in adipocytes which we need for the BMAd study (Sztalryd and Brasaemle, 2017).

PLIN1 is present in at least three isoforms. It is a marker of adipocyte differentiation and participates in regulating cell lipid hydrolysis (Westhoff et al., 2017). Because of its wide existence in lipid droplets and special localization on the surface of lipid droplets, it could be considered an advantageous biomarker for the identification of BMAds in bone tissue samples (Craft et al., 2019). There are at present known isoforms, Perilipin-1 A and B. Both are encoded by a single-copy gene and are the consequence of differential splicing events (Tansey et al., 2004).

1.5. Micro-computed tomography

Depending on the goal of the research, different imaging techniques are available for bone study. For example, imaging diagnostics, through X-rays, dual-energy X-ray absorptiometry (DEXA), Ultrasonography, computed tomography (CT), and magnetic resonance imaging (MRI), provide methods for diagnosis and characterization of fractures and semi-quantitative and quantitative methods for assessing bone consistency and strength (D'Elia et al., 2009). Non-invasive techniques can provide structural information about bone, beyond simple bone densitometry. One of the different studies (Genant et al., 2008) shows that bone mineral density (BMD) only partly explains bone strength because it is not able to capture all aspects of bone strength, which is affected also by microstructure, qualitative properties of bone matrix, and rate of bone metabolism. Methods for assessing the microstructure of trabecular bone non-invasively in rodents include high-resolution CT (HRCT), micro-CT (μCT), high-resolution MRI (HRMRI) and micro-MR (μMR). Volumetric Quantitative CT (vQCT), HRCT and HRMRI are generally applicable *in vivo*; μCT and μMR are

principally applicable *in vitro*. Some methods are available for humans *in vivo*, for example, peripheral ultrasound, DEXA, peripheral QCT and MRI. (HK et al., 2008; Campbell and Sophocleous, 2014).

μCT is a high-resolution imaging modality that is capable of analyzing bone structure with a voxel size on the order of 10 μm. It allows the three-dimensional (3D) nature of the bone structure to be visualized and numerous bone structural parameters to be quantified with a high degree of accuracy. With the development of i*n vivo* μCT, where disease progression and treatment can be monitored in a living animal over a period, such modality has become a standard tool for preclinical assessment of bone architecture during disease progression and treatment. The same parameters for data acquisition and analysis methods must be used for meaningful comparison between μCT studies. Scan and analysis methods for trabecular and cortical bone are covered for the femur and tibia of rodents. However, other small animals can be used, as well, even non-biological materials. Because of the limited field of view and high radiation dose, *in vivo* applications of μCT are limited to preclinical animal studies. Standard scan settings and, analysis regions must be used to compare data from different studies (Campbell and Sophocleous, 2014).

In vivo

Although the advantages of *in vivo* μCT scanning, such as the ability to follow a single subject longitudinally are impressive, it also has its limits. *In vivo* scanning requires the subject to be anaesthetized for the duration of the scanning protocol which can become costly and depending on the frequency of the anaesthesia, might affect animal welfare. Very high-resolution *in vivo* imaging is also not the most optimal option when repeatedly scanning animals due to the extensive scan time and dose of ionizing radiation to the animal that is associated with these techniques (Longo et al., 2017).

Ex vivo

Ex vivo μCT instruments allow for higher spatial resolution, longer scan times as the dose to the sample is not of concern, better signal-to-noise ratios, and therefore better images. *Ex vivo* systems have typically been used for most applications outside of a living animal. One of the common *ex vivo* applications is imaging fine trabecular bone of mice and rats for osteoporosis.

While *ex vivo* scanning of isolated bones can only be analyzed at a one-time point, *in vivo* scanning allows for less time-sensitive scanning protocols and the use of smaller voxel sizes and rotation steps to acquire the highest quality image (Longo et al., 2017).

In *ex vivo* μCT scanners, there is no need to have to be concerned about any physiological monitoring, or dose to the animal, and can more securely mount the sample to avoid movement. This means that the sample stage can rotate while the heavy x-ray source and camera remain stationary. Rotating a small sample and stage in an *ex vivo* scanner has two advantages; the first is that a higher degree of rotational accuracy can be achieved which translates into a better 3D resolution in the reconstructed image, and the second is the ability to change the distance between the source and sample by translating the rotational stage and, in some systems, the distance between the source and the detector giving control of the geometric magnification.

μCT could be considered a standard tool for the measurement and visualization of bone structure. Its modality allows the 3D nature of the bone structure to be visualized and numerous bone structural parameters to be quantified with a high degree of accuracy. One of the top advantages of using *ex vivo* tissues is the ability to perform tests and measurements that would otherwise not be possible or ethical in living subjects.

2. MAJOR AIMS AND HYPOTHESES

2.1. AIMS

Due to the current limitations for studying BMAds in the colour-based H&E staining method, we proposed the following aims for this project:

Aim 1: To develop and optimize a method for the identification of BMAds in bone tissue sections by immunostaining of adipocyte-specific protein PLIN1. As PLIN1 proteins localize to the surface of neutral lipid deposits, we expect a ring-like structure to highlight the presence of a single, large lipid droplet in BMAds (Dalen et al., 2013). We aim to compare a novel IHC-based method to a method based on H&E staining developed previously in our research group (unpublished).

We hypothesize that IHC can be a more specific method to identify BMAds. We will mainly focus on biomedical imaging-related methodological development. IHC-based identification and quantification of BMAds will be compared with the identification of BMAds by conventional H&E staining by using ImageJ and other software-based tools.

Aim 2: To use the PLIN1-based IHC method to identify and quantitate BMAds in rat long bones.

We will evaluate if the newly developed methodological approach would be possible to use in bone samples collected from *in vivo* animal experiments. If the IHC-based detection of BMAds will be achieved, the second aim of this thesis is to apply this method to rat bone tissue samples obtained from normal and obese animals. We aim to investigate if the amount of BMAds is altered in obesity and how exercises affect the results.

2.2. HYPOTHESES

We hypothesize that the IHC method will be better in identifying BMAds in bone tissue histological samples than the conventional H&E method. The optimized protocol of IHC should be a more specific way that can identify adipocytes with special fluorescence staining compared to simple histological H&E staining. H&E staining for

adipocytes is only an “empty area”, like “a negative staining”, while IHC is positive detection. Furthermore, the optimized ex vivo IHC quantitative analysis method will be suitable for immunostaining of bone tissue samples. We hypothesize that the amount and size of BMAds may be different in lean and obese animals.

3. MATERIALS AND METHODS

3.1. Animals

Sprague Dawley (SD) rats (16-week-old) were obtained from Central Animal Laboratory, University of Turku, and the tissue collection from naïve rats has been approved by the local ethical committee. Femur and tibia were processed in steps as shown below in Figure 4 to get final formalin-fixed paraffin-embedded (FFPE) samples. First, 10% neutral buffered formalin was used for formalin fixation overnight. Bone tissues were decalcified in Ethylenediaminetetraacetic acid (EDTA, 1mM, pH 9.0) solution for 16 days at room temperature with shaking to make sure the decalcification solution was flowing around the bone. During the process of decalcification, the solution was changed every 2 to 3 days. The latter steps (paraffin-embedding and sectioning) were done with a thickness of 4 µm longitudinally by the Histology Core Facility, the University of Turku for FFPE following a sequence.

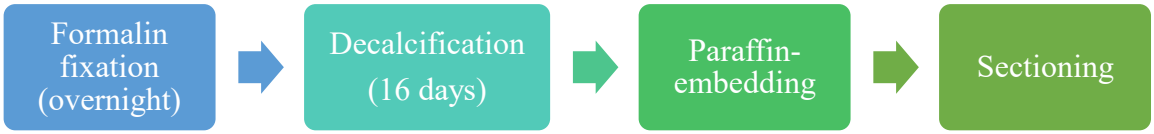

Figure 4. The workflow of sample preparation.

For aim 2, the diet-induced and exercises rat model was referred to collaboration (Dr Jarna Hannukainen) who holds the ethical permit for the study which was used at the later period of the project for study purposes. Eight-week-old rats were subjected to a 12-weeks CTRL (control group with standard-chow-diet), HFD (high-fat-diet) or HF-EX (high-fat-diet and exercise), then sacrificed at the age of 20 weeks (n=2 per group) which is shown in Table 1. CTRL was maintained in standard-chow-diet, obesity was induced by HFD intervention, and another group (HF-EX) was subjected to voluntary exercises as an exercise wheel was put inside the cage. Long bone tissue samples (tibiae) were collected for the study and analysed by µCT to obtain information on bone histomorphometry (Kim et al., 2018). Then, tibias were decalcified and processed for histology as presented in Figure 4. BMAds were quantitated from several regions of interest in the bone marrow cavity using IHC for PLIN1.

Table 1. Animal experiment design. CTRL=control group, HFD=high-fat-diet, HF-EX=high-fat-diet and exercise.

Animal groups	Intervention starts (weeks)	Intervention (12 weeks)	Scarification (weeks)
CTRL	8	standard-chow-diet	20
HFD	8	high-fat-diet	20
HF-EX	8	high-fat-diet and exercises	20

3.2. Haematoxylin and eosin staining

Sections from bone tissue were histologically stained with H&E by the Histology Core Facility, the University of Turku for FFPE following a sequence. All the slides were first examined under a brightfield Olympus CH30 Microscope (Olympus, Hamburg, Germany), and then scanned with the Pannoramic P1000 slide scanner (3DHistech, Budapest, Hungary) to scan the whole slide.

3.3. Immunohistochemistry

IHC staining was initiated by material selection (potential antibodies and robust positive and negative controls), and then, the trial test was run with controls for optimization and validation.

A series of testing and optimization was needed at the beginning of the project. IHC was applied to samples for trial testing at the beginning of the project to develop a reproducible IHC protocol for FFPE suitable for bone tissue sections. Figure 5 below shows the general workflow of the IHC process.

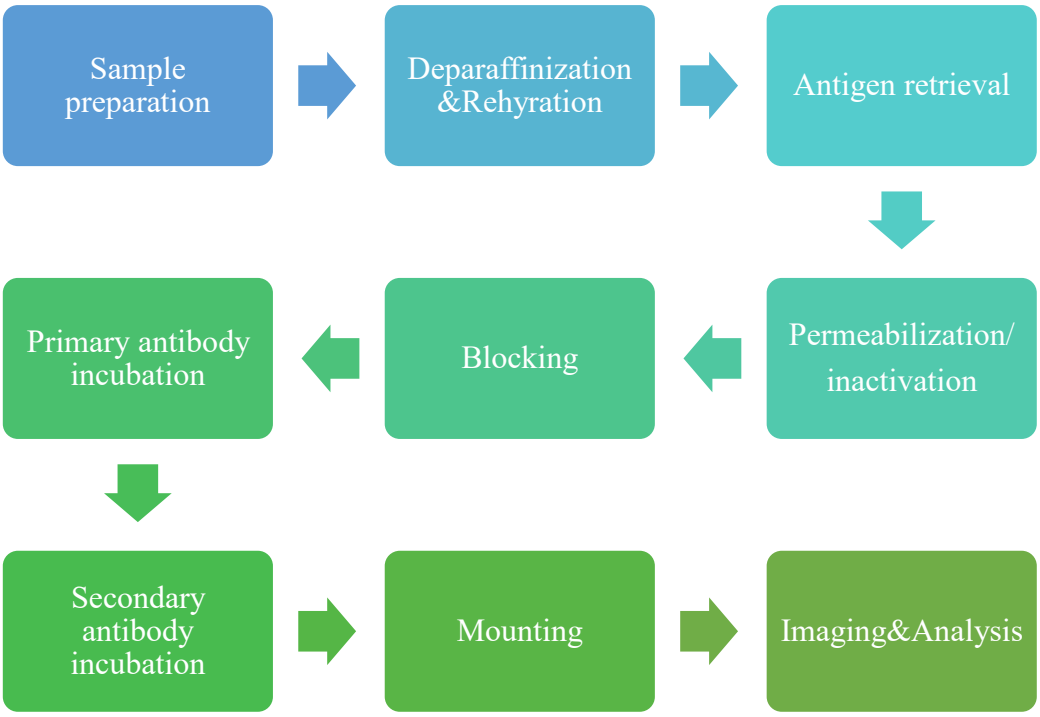

Figure 5. General workflow of IHC process.

Sections were put in the Memmert BE400 incubator (Memmert, Germany) for 1 hour at 50 °C to melt paraffin and to improve tissue adhesiveness. Sections were deparaffinized and serially rehydrated after that, and antigen retrieval (AR) steps were followed up by using heat-induced epitope retrieval (HIER) with Tris-EDTA buffer (10 mM Tris Base, 1 mM EDTA Solution, 0.05% Tween 20, pH 9.0). 0.1% Triton X-100 in Tris-buffered saline (TBS) was used for permeabilizing the cells. Nonspecific binding was blocked by incubating the slides in 10% normal goat serum in 0.1% Tween-20, 20 mM Tris, pH=7.4 in TBS (TBST) solution at room temperature (RT). Anti-PLIN 1 1/500 (detailed information is described in Table 2 below) was used as a primary antibody diluted in 1% normal goat serum in 0.1% TBST to the section, sections were incubated overnight at 4°C.

Table 2. Detailed information on used Abs in the experiment.

Name	Target	Target species	Clonality	Concentration (original)	Proper citation
Perilipin 1 Polyclonal Antibody made in rabbit	Perilipin 1	Mouse, Rat	Polyclonal	1 mg/mL	(Thermo Fisher Scientific Cat# PA1-1051-A555, RRID: AB_2723454)
Goat anti-Rabbit IgG (H+L) Cross-Adsorbed Secondary Antibody, Alexa Fluor 594	IgG	Rabbit	Polyclonal	2 mg/mL	Thermo Fisher Scientific, catalog # A-11012, RRID AB_2534079).

0.1% TBST was used for washing before and after Alexa Fluor 594 1/1000 (detailed information is described in Table 2 above) secondary antibody incubation (diluted in 1% normal goat serum in 0.1% TBST) in a dark environment. Vector TrueVIEW (Vector Laboratories, USA) reagent was used to reduce autofluorescence in the background. After washing in TBS buffer, slides were mounted with VECTASHIELD Antifade Mounting Medium with DAPI (Vector Laboratories, USA) and placed with the coverslip (#1.5 glass).

Zeiss AxioImager (Zeiss, Germany) was used for the first stage of quality checking and manual analysis. Once the quality of staining was ensured by testing different parameters, the Panoramic Midi fluorescence slide scanner (3DHistech, Budapest, Hungary) was applied to scan the full field of tissue, for the next stage of analysis by using the following setting in Table 3 below.

Table 3. Setting for scanning.

Scanning mode	Auto	
Channel	TRITC-43	DAPI=ZERO
Exposure time (ms)	1000	300
Bit depth	8	
Image quality	Custom (PNG)	
index	2	0

The final analysis was mainly carried out by ImageJ (Schindelin et al., 2012) to quantify BMAds and analyse various morphological parameters.

3.3.1. Optimization

The possibilities of optimization of IHC are listed addressing specific issues associated with the staining of hard and matrix-rich bone tissues. The optimization can be applied in both the preparation of samples and during the IHC staining process.

For IHC, many factors can affect the quality of the sample and the staining, which include the time length for warming up in deparaffinization steps. Other steps for optimization include the staining protocol, the buffer and equipment chosen for antigen retrieval, and the choice of counterstaining/mounting media.

Several steps needed to be considered to ensure the quality of staining (Table 4).

Table 4. List of possible factors that affect the quality of the sample and staining outcome.

Factors	Consideration
Type of sample	Fixed vs frozen
Antigen retrieval	Heat-induced epitope retrieval (HIER) Proteolytic-Induced Epitope Retrieval (PIER) Enzyme-Induced epitope retrieval (EIER) Room Temperature Epitope Retrieval (RTER)
Primary antibody	Monoclonal vs polyclonal
Blocking	Temperature, pH, dilution, incubation time
Secondary antibody	Species, label type
Labelling	Chromogenic, enzymatic, or fluorescent
Counterstaining	Chromogenic or fluorescent
Analysis	Direct evaluation by eyes, use of microscopes, software-based analysis
Controls	Only secondary antibody, antigen-positive tissue, isotype control

3.3.2. Antigen retrieval (AR)

AR was used to enhance the ability of a primary antibody to bind a specific epitope in FFPE tissue. The AR technique of boiling FFPE tissue sections in water was a highly effective method to render IHC staining on FFPE tissue sections(Goodwin et al., 2018; Shi and Taylor, 2014; Wang-Rodriguez, 2002).

In the starting, both HIER and EIER methods were tested for restoring the immunoreactivity of an epitope. HIER with 10 mM sodium citrate (SC) was tested at the beginning of the experiment, but it highly destroyed the morphology of the tissue. Subsequently, RTER with 0.1M formic acid (FA) was tested, but it showed poor signals when checked afterwards. After multiple attempts, from incubation time to mounting media choosing, optimization of the index and testing of various buffer solutions were done. The HIER method with 1mM Tris-EDTA buffer was chosen at the end for better tissue morphology that showed low efficacy of destruction of tissue and gave also good signals.

A summary of the experiments with different AR methods of destruction in IHC protocol is listed in Table 5 below.

Table 5, Experiments with different antigen retrieval methods in IHC protocol.

AR	Solution/ Buffer	Pre-warm time (min)	Method	Heating (microwave)
HIER 1	SC	10	Microwave	800w3min+320w7min
HIER 2	SC	10	Microwave	800w3min+160w7min
RTER 1	FA	60	RT 20min	No heating
HIER 3	SC	60	Microwave	800w3min+160w7min(ice)
HIER 4	SC	60	Microwave	800w3min+160w7min(ice)
HIER 5	Tris-EDTA	60	Microwave	800w1min+160w7min(ice)
HIER 6	Tris-EDTA	60	Microwave	800w1min+160w14min(ice)

3.3.3. Autofluorescence (AF)

Both chemical-based and quencher autofluorescence reduction methods were tested. Chemical-based treatment of 10 mM CuSO4 in 50 mM NH4Cl buffer (pH 5) or 0.3% Sudan Black B (SBB) in 70% ethanol were first tested to reduce AF in FFPE rat bone tissue sections. For quencher, Vector TrueVIEW reagent was tested.

3.4. Micro-computed tomography

Bone samples were collected before μCT scanning. The scans of rat tibiae were performed on the Skyscan 1272 (Bruker Corporation, USA) μCT scanner with scanning parameter settings are shown below in Table 6.

Table 6. Settings for μCT analysis of rat tibiae.

Parameter	Value
Resolution	10 μm
Stage height	66 mm
X-ray filter	Aluminium, 0.5 mm
Camera	2452 x 1640 pixels
Rotational step	0.4 degree
Scanning mode	180-degree rotation
voltage	75Kv

Calibration was done with a phantom of a 4 mm diameter. Images from scanning were reconstructed in NRecon (version:1.7.5.6) and exported for the transaxial rotation step in Dataviewer (version:1.5.6.5). With the final rotated dataset of the transaxial plate, CTAn (version:1.19.10.2+) was used for volumetric and BMD analysis. The contoured regions of interest (ROI) were selected from CT images covering 200 slices (2 mm) (between green lines in Figure 6 A) for the trabecular region 230 slices (230 mm) from the growth plate (orange line in Figure 6 A). And for the cortical region, 100 slices (1 mm) (between blue lines in Figure 6 A) were selected 50% down of the whole length from the growth plate. CTvol (version 2.3.2.1) was used at the end for the 3D structure visual presentation.

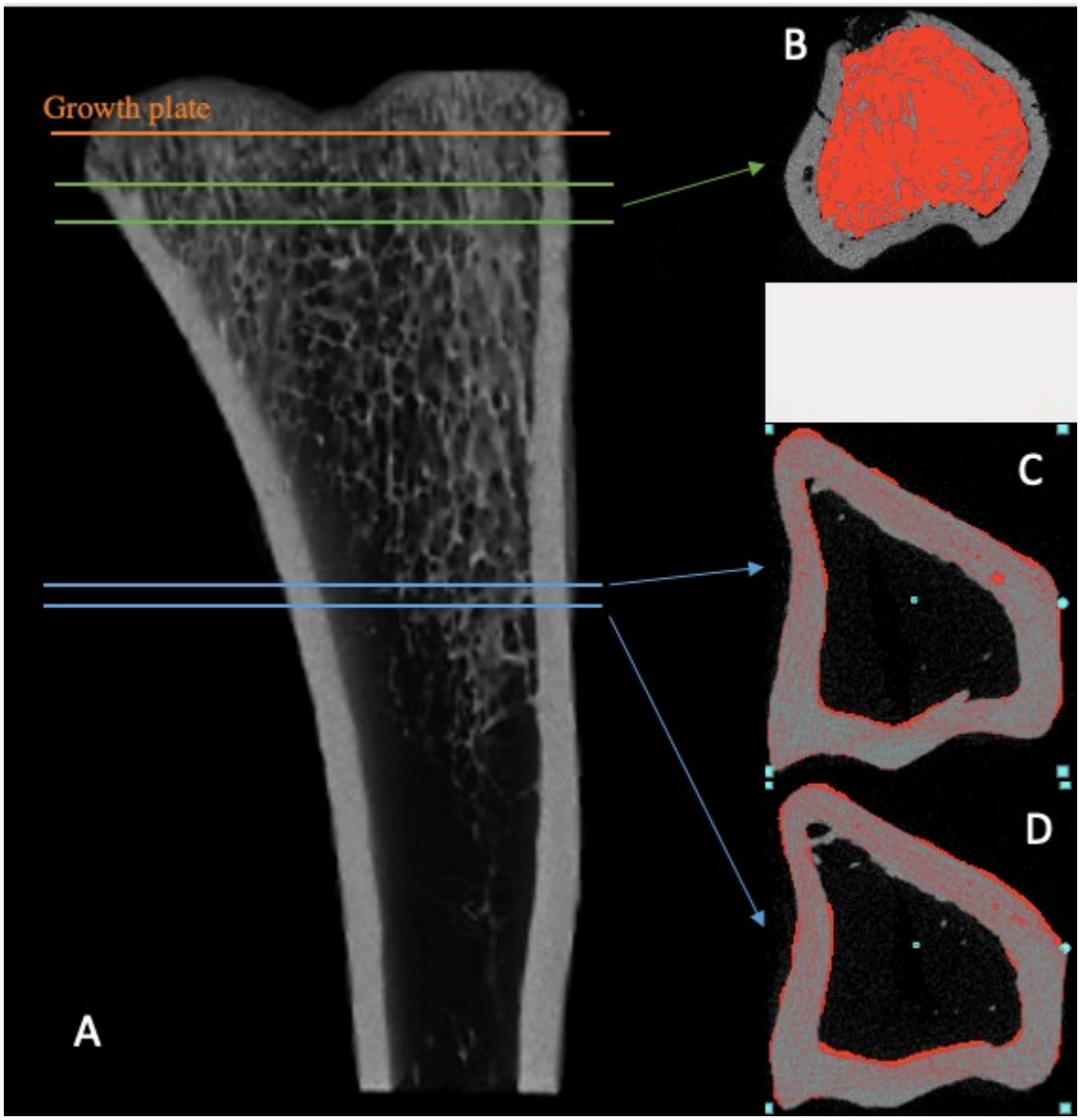

Figure 6. Example of ROI selections. A) Partial view of bone. B) Example of ROI (red area in middle) of trabecular bone. C) Example of ROI (red area) of cortical bone on the top layer and D) Example of ROI (red area) of cortical bone on the bottom layer.

3.5. Summary of material and methods

Figure 7 below presents the summary of the material and methods. Multiple possible optimizations were conducted during the planning to processing stages.

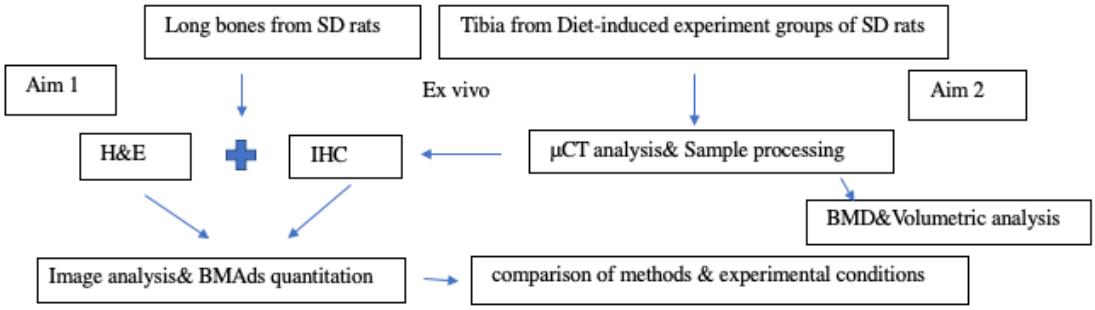

Figure 7. Overview of research design.

4. RESULTS

4.1. Immunohistochemistry

4.1.1. Antigen retrieval method

During the trial, different types of problems emerged. One of the difficulties appeared during the AR step. Many methods can be used for achieving successful AR in FFPE tissue, of which RIER and HIER were both tested during the AR step with SC and FA buffers. In the end, the HIER method with Tris-EDTA buffer was the best combination with better tissue morphology that showed low efficacy of destruction of tissue and gave also good signals.

A summary of the experiments with different AR methods in the IHC protocol is listed in Table 7 below. Tissue damage was estimated visually, "high" in Table 7 means more than 50% of the tissue detached from the object's glass. The fluorescence signal was observed under the microscope. From the results presented in Table 7, we can conclude that HIER 6 is the best of the AR methods tested, with the lowest tissue damage and detectable fluorescence signal.

Table 7. Summary of experiments with different antigen retrieval methods in IHC protocol.

AR	Buffer	Pre-warm time (min)	Heating method	Tissue damage	Fluorescence signal
HIER 1	SC	10	Microwave 800w3min+320w7min	High	Low
HIER 2	SC	10	Microwave 800w3min+160w7min	High	Low
RIER 1	FA	60	RT 20min	Low	Low
HIER 3	SC	60	Microwave 800w3min+160w7min (ice)	Promising	Low
HIER 4	SC	60	Microwave 800w3min+160w7min (ice)	Low	Some
HIER 5	Tris-EDTA	60	Microwave 800w1min+160w7min (ice)	Low	Ok
HIER 6	Tris-EDTA	60	Microwave 800w1min+160w14min(ice)	Low	Ok

4.1.2. Antibody concentration

To find the suitable dilution of antibody which shows a significant signal with the lowest concentration, serial dilution experiments were applied for anti-PLIN1. We tried with 1/250, 1/500, 1/1000 and 1/2000 serial dilution (Figure 8) for primary Ab and 1/500 was the lowest dilution which showed enough signal for observation and image analysis. Based on the fluorescence signal under a microscope, we chose 1/500 (2 µg/mL) for primary anti-PLIN1 and 1/1000 (2 µg/mL) for secondary Alexa Fluor 594.

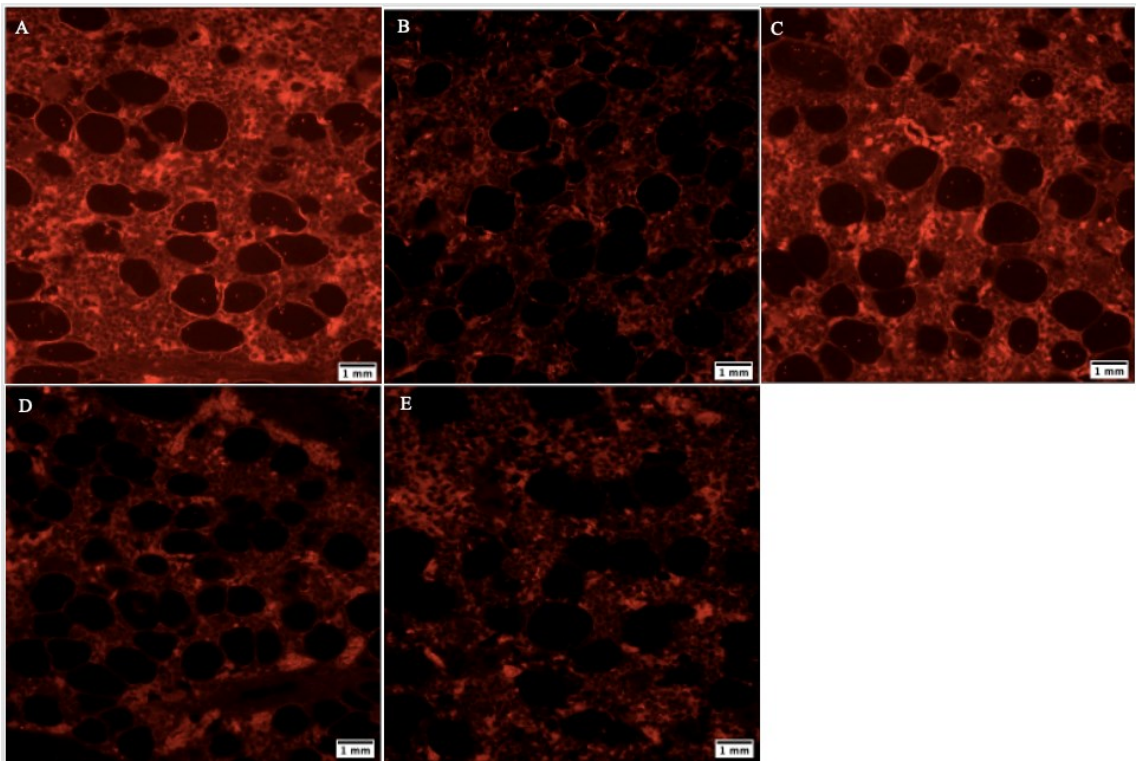

Figure 8. Serial dilution experiments of anti-PLIN1. A) 1/125, B) 1/250, C)1/500, D) 1/1000, E) 1/2000.

All the tested antibodies with different dilutions in experiments for optimization of IHC protocol are listed in Table 8 below.

Table 8. Experiments with different Abs and dilution for optimization of IHC protocol. (AF=autofluorescence)

Primary antibody	1st dilution	Secondary antibody	2nd dilution	AR	Fluorescence Signal
Anti-PLIN1	1/500	Alexa Fluor 488 goat anti-rabbit	1/500	HIER 4	AF
-	-	-	-	HIER 4	AF
Anti-PLIN1	1/500	Alexa Fluor 594 goat anti-rabbit	1/1000	HIER 4	AF
Anti-PLIN1	1/500	Alexa Fluor 594 goat anti-rabbit	1/2000	HIER 5	AF
Anti-PLIN1	1/500	Alexa Fluor 594 goat anti-rabbit	1/1000	HIER 5	High
Anti-PLIN1	1/500	Alexa Fluor 594 goat anti-rabbit	1/1000	HIER 6	High
Anti-PLIN1	1/125	Alexa Fluor 594 goat anti-rabbit	1/1000	HIER 6	High
Anti-PLIN1	1/250	Alexa Fluor 594 goat anti-rabbit	1/1000	HIER 6	High
Anti-PLIN1	1/500	Alexa Fluor 594 goat anti-rabbit	1/1000	HIER 6	High
Anti-PLIN1	1/1000	Alexa Fluor 594 goat anti-rabbit	1/1000	HIER 6	Low
Anti-PLIN1	1/2000	Alexa Fluor 594 goat anti-rabbit	1/1000	HIER 6	Low

4.1.3. Autofluorescence reduction

We tested also with only new hardening mounting media (VECTASHIELD Vibrance Antifade Mounting Medium with DAPI) VEC.H-1800-2) to compare results with other chemical-based and quencher AF reduction methods (Schnell et al., 1999). In the experiment, both Alexa Fluor 594 and 488 channels were checked and compared together to find the possible usable colour signal channel. We have found that tissue treatment of $CuSO_4$ buffer is a good approach to eliminate tissue AF and background

while preserving the specific fluorescence hybridization signals compared with SBB and new mounting media (Figure 9). Using 10 min treatment after secondary antibody shows better results (see Table 8) after retreated with different periods and combined with antibodies.

Next, we compared the effectiveness of an autofluorescence quencher TrueVIEW (Vector Laboratories, Burlingame, CA, USA) in parallel with other available AF reducing products from commonly autofluorescence-emitting channels on bone sections (Alexa Fluor 594/594nm and Alexa Fluor 488/488 nm). No specific immunostaining was conducted. images from Figure 9 highlight the results.

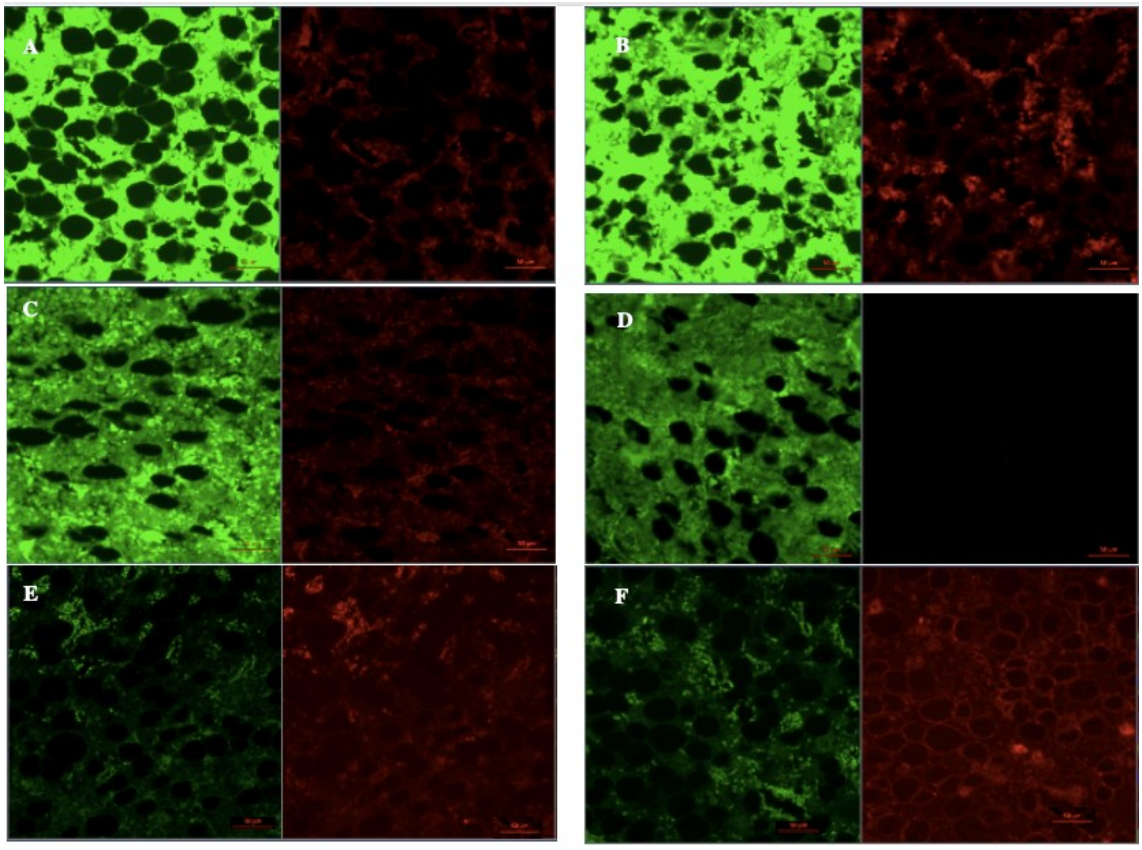

Figure 9. Different AF reduction methods comparison on common autofluorescence-emitting channels A) only VECTASHIELD LS-J1033, B) Only VECTASHIELD H-1800, C) 0.3% SBB+ VECTASHIELD H-1800 and D) CuSO4+VECTASHIELD H-1800, E) Vector TrueVIEW treatment comparison negative control with only anti-PLIN1 and F) 1/500 anti-PLIN1 and 1/1000 Alexa Fluor 594. All images were acquired under identical conditions (including microscope objective=20x and exposure times=400ms).

We could say that quencher TrueVIEW can reduce the total reduction of the tissue AF while maintaining true fluorescent signals. The summary of AF reduction experiments is shown in Table 9.

Table 9. The summary of AF reduction experiments. LS-J1033 and H-1800 are different VECTASHIELD products mentioned before in Figure 9. Methods were applied either before or after using the antibody.

AR	Treatment	Time (min)	Green channel AF	Red channel AF	Use of antibody
HIER1.3	Only LS-J1033	-	Strong	Weak	-
HIER1.5	Only H-1800	-	Strong	Some	-
HIER1.5	SBB+ H-1800	20	Strong	weak	-
HIER1.5	CuSO4+ H-1800	10	Some	Almost none	-
HIER1.5	CuSO4+ LS-J1033	30	Some	Little	-
HIER1.5	CuSO4+ LS-J1033	50	Some	Almost none	-
HIER1.5	CuSO4+ LS-J1033	70	Some	Little	-
HIER1.5	CuSO4+ LS-J1033	90	Some	Little	-
HIER1.5	CuSO4+ H-1800	10	Some	-	Before
HIER1.5	CuSO4+ H-1800	10	Little	-	After
HIER1.5	TrueVIEW kit	5	Almost none	-	After

We found that our samples based on all the following optimized of each step for the IHC protocol below in Table 10 show the best results.

Table 10. The summary of optimized IHC protocol.

Steps	Details
Sample	FFPE
AR	HIER (Tris-EDTA) 800w1min+160w14min (ice) microwave
Primary antibody	Rabbit anti-rat PLIN1 1/500
Secondary antibody	Alexa Fluor 594-conjugated goat anti-rabbit IgG 1/1000
AF reduction	TrueVIEW: endogenous fluorophore quenching
Counterstaining &mounting	VECTASHIELD LS-J1033
Imaging	ZEISS Axio Imager
Scanning	Panoramic Midi fluorescence slide scanner
Processing	CaseViewer
Analysis	ZEN 2(blue edition) &ImageJ

4.2. Region of interest selection for IHC

Region of interest (ROI) was standardized by following steps. For the distal femur (see Figure 10 A), 1 mm^2 square (1mm x 1 mm) was drawn 2 mm higher up from the most protruding area of the growth plate for the trabecular region (see Trab 1 in Figure 10 A) avoiding artefacts or blur region. Then another 3 mm was measured proximally from the selected trabecular selection. Another 1 mm^2 square was drawn for the bone marrow region (see BM 1 in Figure 10 A). At the same level, two 0.25 mm^2 squares were drawn to get cortical regions, one on left and one on the right side, they are negative controls. For proximal tibia (see Figure 10 B), 1 mm^2 square (1 mm x 1 mm) was drawn 3 mm distally from the most protruding area of the growth plate for the trabecular region (see Trab 2 in Figure 10 B) which needs to avoid artefact or blur region. Then another 4 mm was measured proximally from the selected trabecular selection. Another 1 mm^2 square was drawn for the bone marrow region (see BM 2 in Figure 10 b). At the same level, 2 squares of 0.25 mm^2 were drawn into the cortical bone area to get cortical regions (see Cort 1 and Cort 2 in Figure 10 b), one on left and one on the right side, they would be negative controls as cortical bone lacks adipocytes and PLIN1.

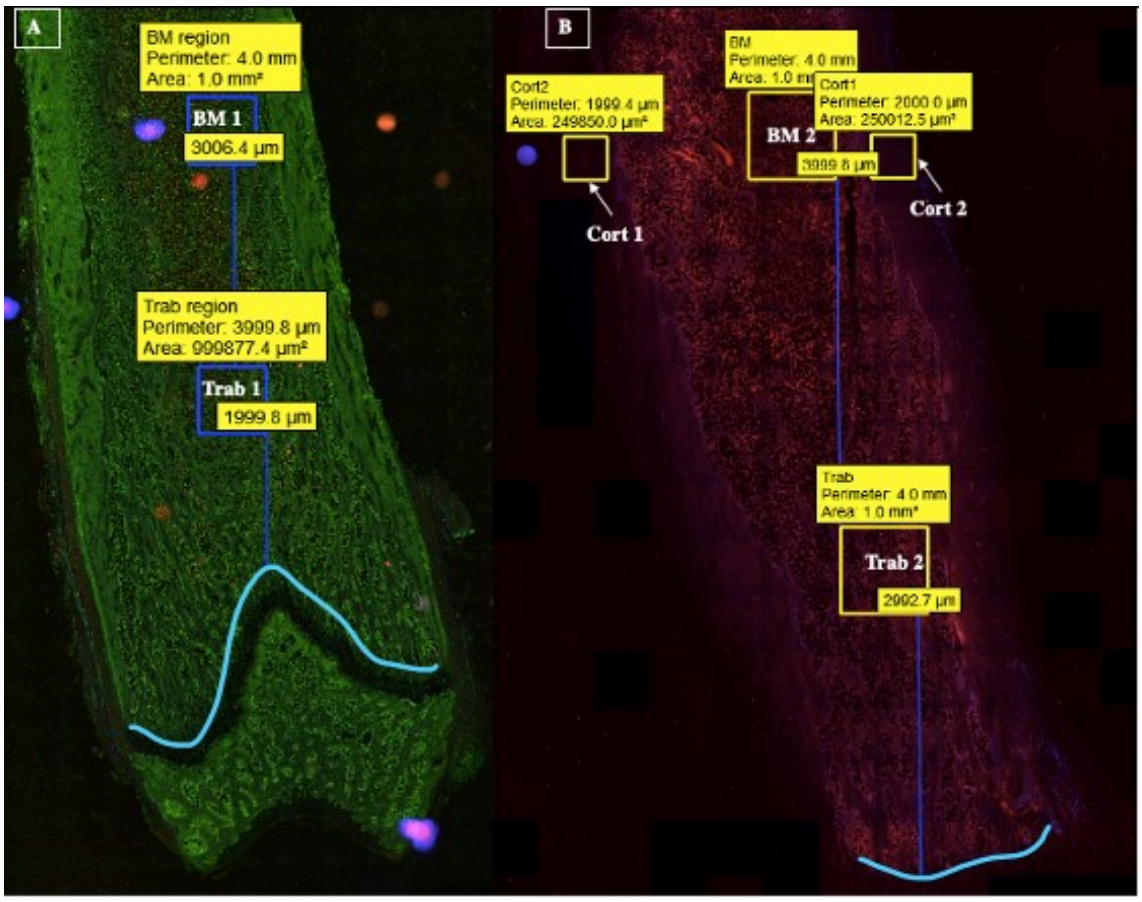

Figure 10. Standardized ROI selection of A) distal femur analysis region and B) proximal tibia. Trab 1 and 2 are examples of trabecular region selection, BM 1 and 2 are examples of bone marrow region selection, and Cort 1 and 2 are examples of cortical region selection. Growth plates were marked with the blue line in the figure. Images were overexposed and false-coloured to highlight anatomical references for the ROI selection.

4.3. Image analysis

Image analyses were done with ImageJ (version 1.0), here is the summary of the analysis process (A detailed script can be found in appendix 1.)

First, cropped tif (Tagged Image File Format) image was opened in ImageJ. Image-Adjust-Threshold was selected and adjusted the value just over 50%, Black Background was selected and applied. Next, Process-Binary-Convert to Mask was selected, followed by Process-Binary-Fill Holes. Then Process-Binary-Watershed was selected. Analyze Particles was set to size = 300-7000; circularity= 0.25-1.00. (0 indicates an increasingly elongated polygon close to a straight line and 1 indicates a perfect circle)

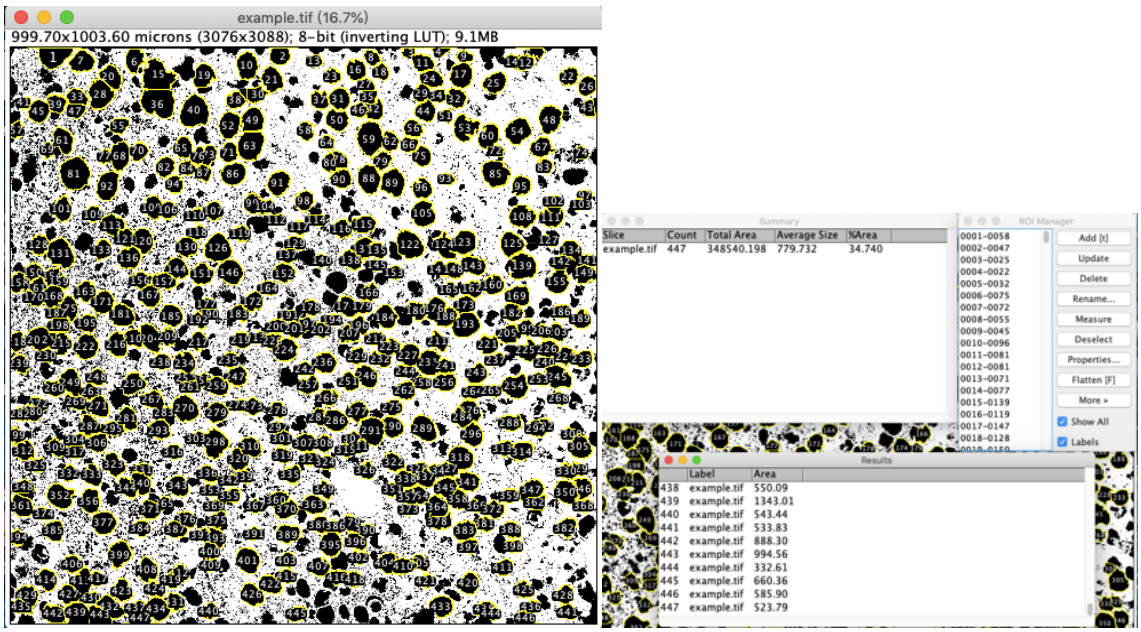

Figure 11. An example of the results from the image analysis process for IHC staining. 447 BMAds were detected in this image with an average size of 779.732 μm ^{2} shown in the summary table.

Adipocytes are usually around 20 to 300 μm in diameter (Stenkula and Erlanson-Albertsson, 2018) which means an area of 300 to7000 μm^2 by using the formula A = πr^2. Figure 11 shows an example of the results from the image analysis process for IHC staining.

During the analysis, single-blind testing of the script was done. As shown in Figure 10, four cropped images of ROI were collected from one slide by one person and counted manually for a total of 5 slides (4 images x 5 slides =20 images in total). Same images were given to another person to use the developed ImageJ script. Then the results were compared, and the correlation between manual and semi-automated count is shown in Figure 12 below. The optimized semi-automated quantitation method was comparable to the manual counting (R=0.959).

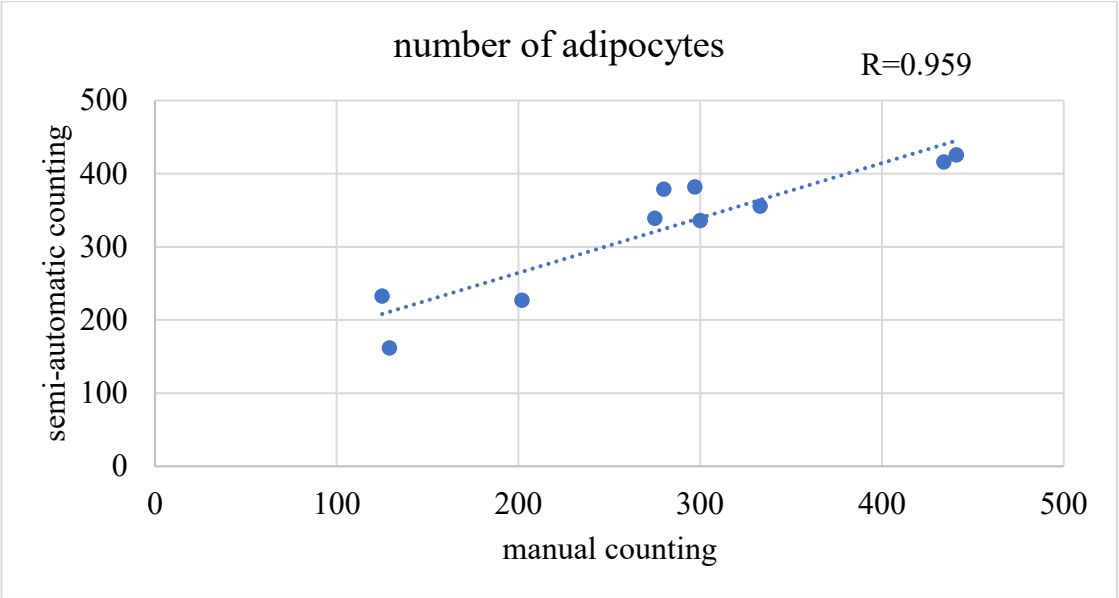

Figure 12. Correlation between adipocyte counts obtained by manual counting and semi-automatic counting.

4.4. BMAds quantitation

By following the same ROI selection, Trab and BM regions were cropped for one slide. For IHC analysis, 3 parallel order FFPE tissue slides were used from a single animal. As mentioned before, three animal groups were used with the number of two in each group. (2 images x 3 slides x 3 groups x 2 animals= 36 images in total)

The number of BMAds was typically 300-500 /mm^2 in the BM region (Figure 13 A) and the size range of BMAds was about 700 to 1000 µm^2 (Figure 13 B).

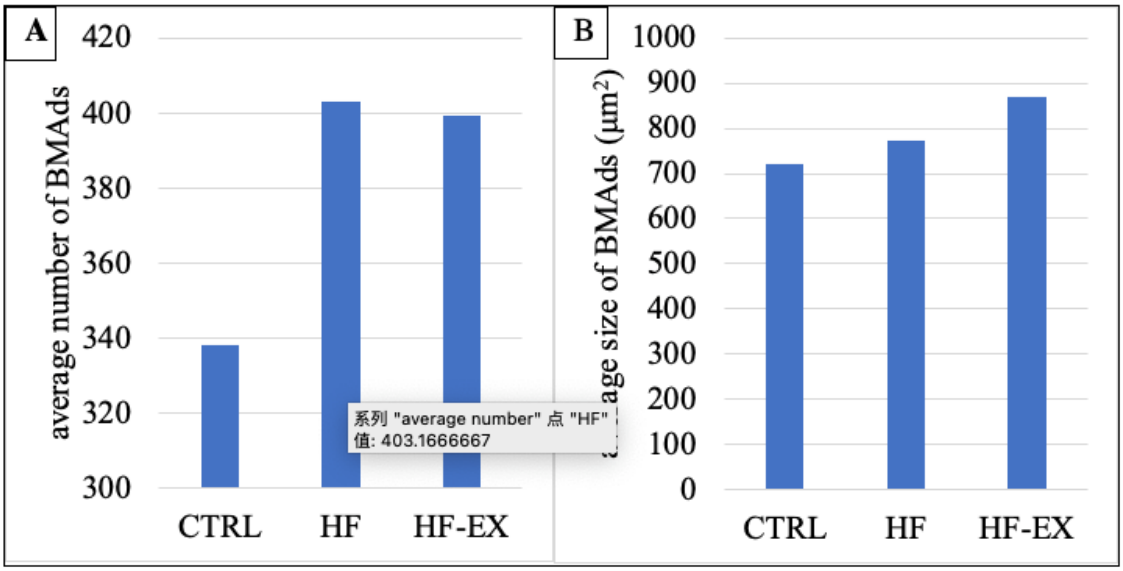

Figure 13. A) Average number of BMAds in BM region and B) Average size (μm^2) of BMAds in BM region in different animal groups.

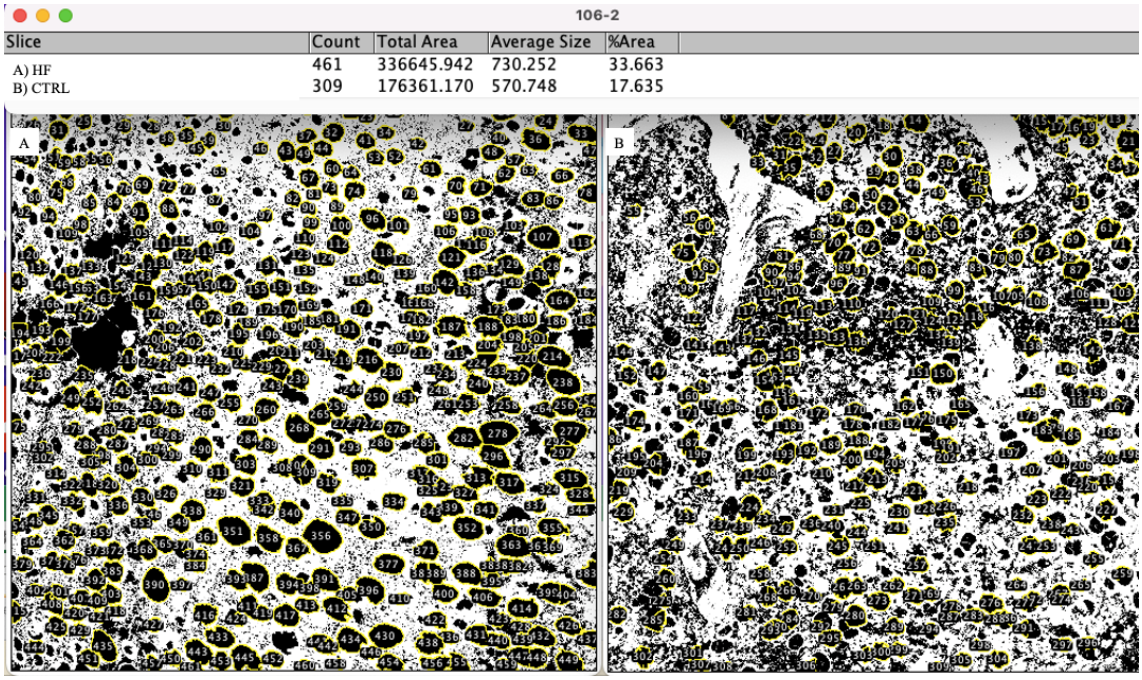

Figure 14. Example comparison in BM region analysis for the number of BMAds and average size (μm^2) of BMAds in A) HFD animal group and B) CTRL (normal chow diet) animal group.

Animals on the HFD had a bigger average size and average number BMAds when compared to animals on a normal chow diet. Exercise tended to reduce the average number BMAds even on the HFD when compared to animals only on the HFD but without exercise intervention. One of the example comparisons in BM region analysis

for the number of BMAds and average size (μm^2) of BMAds in HFD and CTRL animal groups are shown in Figure 14.

4.5. Micro-computed tomography

The fat fraction was measured with EchoMRI as shown in detail in Table 11 below.

Table 11. EchoMRI measurements of rats.

Sample	weight (g)	Lean weight (g)	Fat mass (g)	Fat-%
CTRL 1	478.3	425.66	38.38	8.02
CTRL 2	495.5	430.82	50.42	10.18
HFD 1	540.5	455.19	69.79	12.91
HFD 2	528	462.28	52.88	10.01
HF-EX 1	592.6	462.03	113.02	19.07
HF-EX 2	660.1	531.13	109.09	16.53

Volumetric analysis of trabecular bone is shown in Figure 15. Animals on the HFD had smaller bone volume (BV/TV) and bone surface (BS), increased trabecular separation (Tb. Sp) and decreased trabecular number (Tb. N) when compared to animals on normal chow. Exercise tended to reduce the total porosity (as shown in Figure 15 C). Both trabecular and cortical BMD was slightly higher in HFD, and HF-EX animals compared to control animals (as shown in Figure 15 D and E). However, statistical analysis was not performed due to N=2, so the result needs to be replicated in a larger study. The 3D structure visual presentation for cortical and trabecular bones below was done by CTvol.

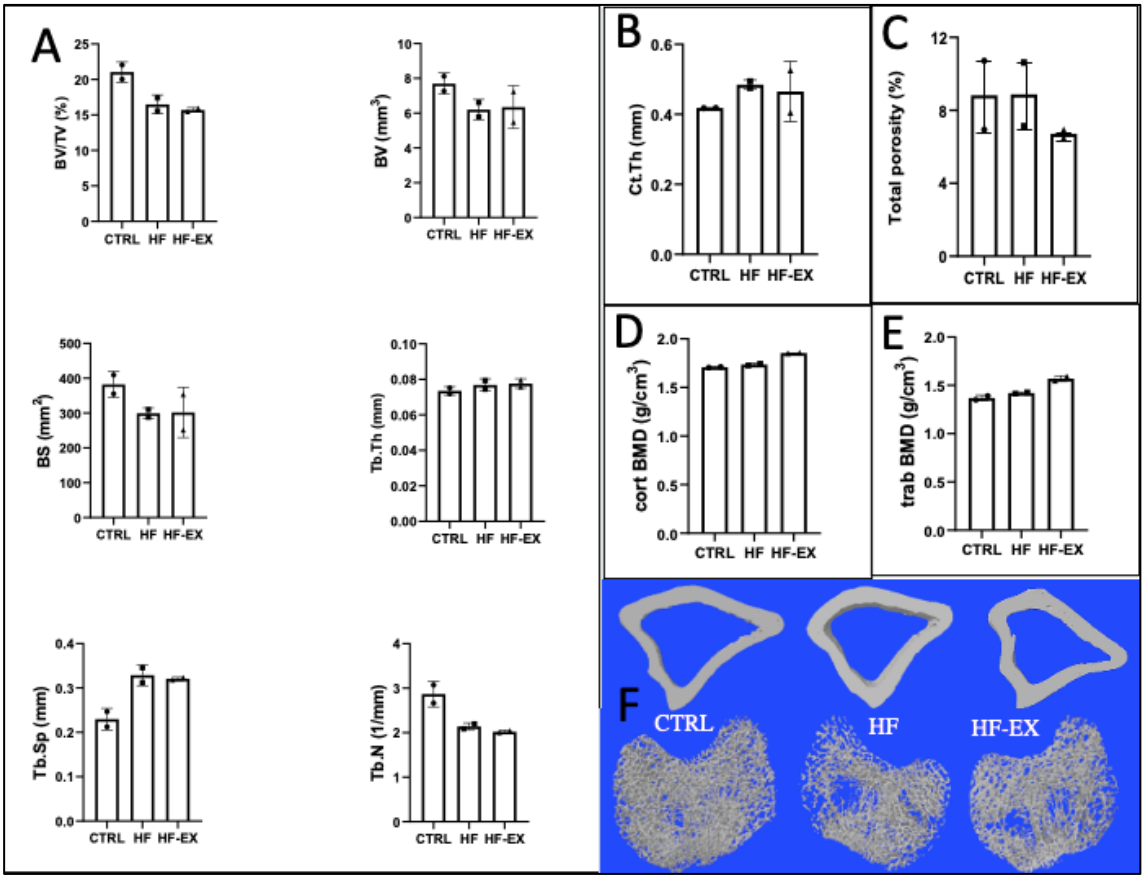

Figure 15. A) Volumetric analysis of trabecular bone; B) and C) volumetric analysis of cortical bone; D) BMD analysis of cortical bone; E) BMD analysis of trabecular bone; F) 3D structure visual presentation CTRL, HFD and HF-EX. (BV/TV=trabecular bone volume fraction; BV=bone volume; BS=bone surface; Tb.Th=trabecular thickness; Tb.Sp=trabecular separation; Tb.N=trabecular number; BMD=bone mineral density; Ct.Th=cortical thickness)

5. DISCUSSION

Extracting the number and size of BMAds in histologically stained bio-images is the major aim of this study. After applying optimal AF reduction treatment to the imaging setup, we noticed that AF was reduced in the BM region. Brightness was increased to make it analysable, as it would not change the size of the object and the intensity analysis was not our main interest. With the final optimized IHC protocol and selected antibodies, morphologically preserved BMAds could be identified easily from the images as intact ring-liked structures (Figure 16).

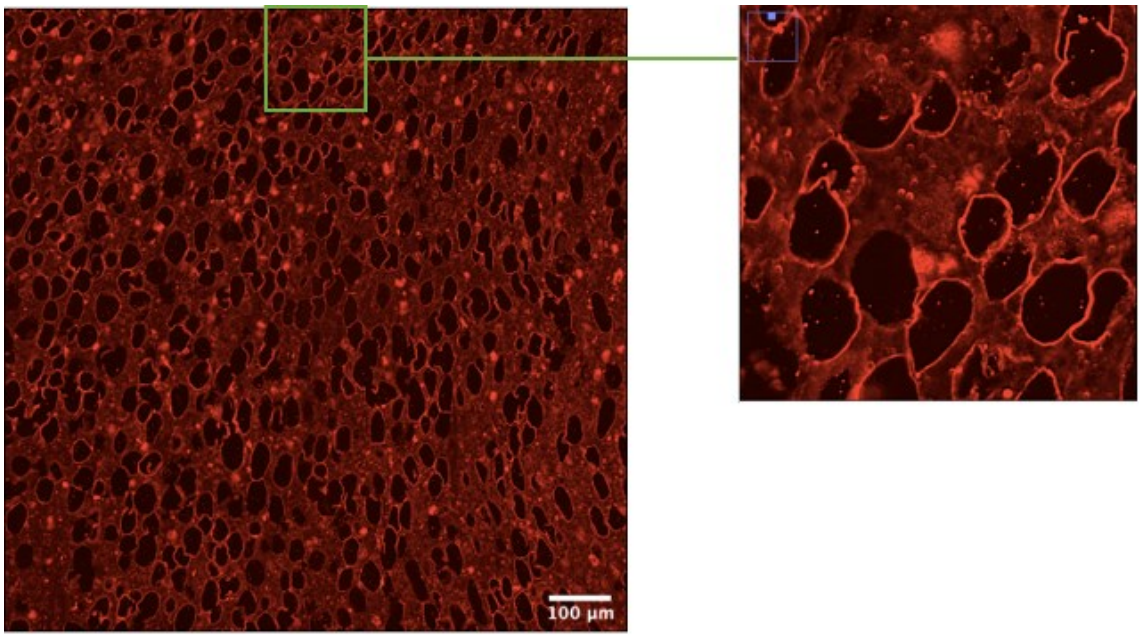

Figure 16. PLIN1 positive staining of BMAds in bone tissue section.

Protocol for the visualization of BMAds in FFPE rat long bone tissue samples using the IHC method was developed and optimized as the aim of the project. As we hypothesised at the start, the sample of IHC would be a better study model compared with traditional H&E staining.

5.1. Optimization of immunohistochemistry

From the *ex vivo* model, we showed an optimized IHC protocol applicable for bone tissue samples which is the major aim of the project. However, histological assessment (sectioning, staining, imaging, and analysis) remains a challenging, time-consuming, and often costly technique.

For preparation, bone tissue as a sample material may affect the quality of tissue sectioning, as the bone has a different hardness ratio (even after decalcification) compared to other organs. FFPE tissues can be stored much longer than frozen ones. Staining time also affects the quality of the sample after AR.

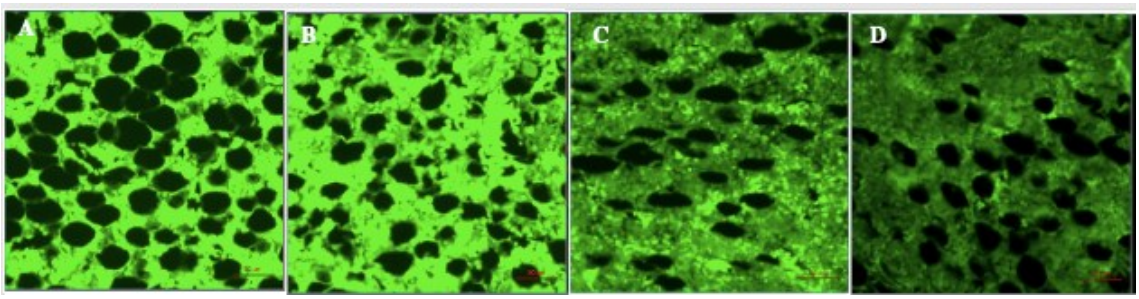

Figure 17. Different AF reduction methods in the green autofluorescence-emitting channel A) only VECTASHIELD LS-J1033, B) Only VECTASHIELD H-1800, C) 0.3% SBB+ VECTASHIELD H-1800 and D) CuSO4+VECTASHIELD H-1800. All images were acquired under identical conditions (including microscope objective=20x and exposure times=400ms).

Interference by AF is one of the major concerns of IF analysis (Oliveira et al., 2010). What we need is a useful technique that reduces AF background without affecting the tissue integrity or directing IF signals in bone sections. Bone tissue showed massive AF in the green channel (488nm) (Figure 17). The phenomenon of fluorescence of bone is primarily due to the collagen itself rather than to incidental substances absorbed into it (Prentice, 1967). But not much fibrous-like structure was seen in our section, but rather small cells which might be pan-cytokeratin and white blood cells inside the marrow being highly AF (Axelrod et al., 2018).

5.2. Quantitation analysis

Individual size measurement of adipocytes is beneficial in the analysis of BMAT, as the changes in total adipose tissue could be due to either an increase in the number or the size of adipocytes. Some radiological imaging does not necessarily report individual size as they are not resolvable in the image, but still highly useful to report adiposity by volume in humans (Wang et al., 2014; Uppot, 2018).

This distinction is critical since the mechanism behind these changes could reveal differences in adipogenic differentiation or metabolic profile. The hematopoietic area is defined either by CD45 (Yeh et al., 2006) positivity in IHC or, morphologically, by

the areas defined by the high density of hematopoietic cell nuclei within the marrow space.

Another significant histological measure for BMAd is the density of adipocytes which is also used to differentiate between adipogenesis and enlargement of the adipocyte due to lipid storage. Adipocyte density varies greatly in the endocortical vs. trabecular regions of the bone (Scheller et al., 2016; Tratwal et al., 2020b)) and, thus, detailed annotation and standardization of the quantified region are paramount. Therefore, we recommend standardizing ROI for quantification analysis as described in previous chapters. In our correlative analysis, the optimized semi-automated quantitation method was comparable to the manual counting (R=0.959).

5.3. Micro-computed tomography

The pilot study showed that with an HFD there are some decreases in percent bone volume, bone surface, and trabecular number but increases of trabecular separation.

μCT can be an applicable method for the volumetric study of bone tissue. On one hand, a bigger group is needed for more accurate results for further data analysis. On the other hand, a longer intervention time of treatments might give a better comparison. More combinations of treatments might also highlight the found out. For example, a possible interstation can be CTRL with EX to show if there would be significant changes for both influenced by low-fat food plus exercise. Exercise tended to reduce the total porosity and increase BMD in both trabecular and cortical bone.

These trends correlate to previously published studies, the same trends were found when comparing bone parameters between HFD and exercise (Horge et al., 2016).

5.4. Final summary

Even though histomorphometry analysis is a beneficial tool to determine the quality of bone, many limitations remain. Histological assessment (sectioning, staining, imaging, and analysis) remains a challenging, time-consuming, and often costly technique.

Besides that, even today, this technique still has relied on the interpretation of a single investigator, so it needs a solid quality control system. The detection of BMAds could be hampered by the close connection of adipocytes in adipocytic areas, making the

separation and adequate counting of clustered adipocytes a big challenge, especially if membranes are not intact (Tratwal et al., 2020b). But compared with H&E images, following the guidance of PLIN1 staining could help in connecting those missing membranes (Figure 18).

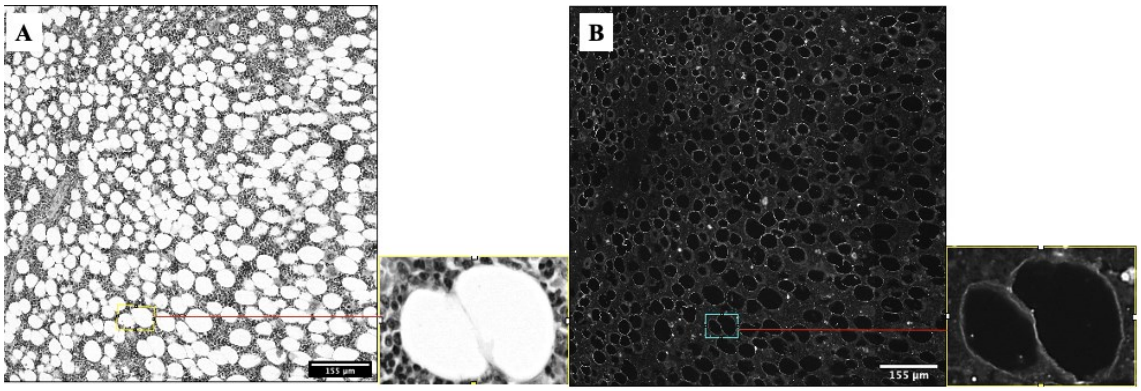

Figure 18. Comparison of BM region staining of A) H&E staining method and B) IHC PLIN1 staining method.

The distinction of adipocytes from small blood vessels could still be a challenge in H&E staining which might need additional immunostaining to discern microvasculature from adipocyte ghosts as a validation step. But in our IHC method, no blood vessels were visible, PLIN1 signal is very specific.

Validation of automatic detection of adipocytes is described in our results. We have performed a correlative analysis, which in a way supports our notion that this ImageJ based method correlates well with the manual count. Based on the intended application of our pilot study, we have successfully shown the reproducibility by testing the script from different biological samples.

Future applications of our method could be improved in different ways. For example, involving deep learning and machine learning for better image analysis methods to resolve our limitations and improve accuracy. In our case, image classification for determining whether it is an adipocyte or other unwanted cells, image segmentation for identifying single adipocytes in images, and so on (Moen et al., 2019). Based on the needs, implementations are developed by us to teach the computer how to do to achieve the goals. It might take some time during the learning process but once the systems have been built up, the image process speed can be faster than the current stage.

6. CONCLUSION

Protocols for the identification and quantitation of BMAds in FFPE bone tissue samples using the IHC method were developed and optimized. In this study, however, a limited number of study groups were tested. Therefore, bigger study groups are needed. Detection of BMAds in bone tissue using this IHC approach could play an important role in experimental samples. This method will have multiple applications in animal studies investigating the biological role of BMAds, and the effects of various physiological and pathological stimuli on BMA. Later, similar IHC methods can be optimized also for human BM samples. This will allow the evaluation of MAT also in human studies by staining BMAds in BM biopsies in the future. Based on the achieved results, the conclusion could be summarized:

1. The final optimized IHC method brings improvement over H&E as it can positively stain BMAds. It can be applied to histological bone tissue sections.
2. The optimized semi-automated quantitation method was comparable to the manual counting. (R=0.959)
3. Based on our preliminary data, the method may be suitable to apply to samples collected from *in vivo* experiments.

ACKNOWLEDGEMENTS

I would like to thank professor Kaisa Ivaska-Papaioannou to let me have the chance to join the research group and finish my master thesis, and my 2nd supervisor M.Sc. Nicko Widjaja for their leadership and support for this project. And my thanks to Jarna Hannukainen from Turku PET Centre for animal-related support and Jorma Määttä from the Institute of Biomedicine for the guidance of μCT related studies.

REFERENCES

Adams, J.E. 2009. Quantitative computed tomography. *European Journal of Radiology*. 71:415–424. doi:10.1016/J.EJRAD.2009.04.074.

Alturkistani, H.A., F.M. Tashkandi, and Z.M. Mohammedsaleh. 2015. Histological Stains: A Literature Review and Case Study. *Glob J Health Sci*. 8:72–79. doi:10.5539/gjhs.v8n3p72.

Attané, C., D. Estè, K. Chaoui, O. Schiltz, N. Reina, and C.M. Correspondence. 2020. Human Bone Marrow Is Comprised of Adipocytes with Specific Lipid Metabolism. doi:10.1016/j.celrep.2019.12.089.

Axelrod, H.D., K.J. Pienta, and K.C. Valkenburg. 2018. Optimization of Immunofluorescent Detection of Bone Marrow Disseminated Tumor Cells. *Biological Procedures Online*. 20:1–13. doi:10.1186/S12575-018-0078-5/TABLES/1.

Balistreri, C.R., C. Caruso, and G. Candore. 2010. The role of adipose tissue and adipokines in obesity-related inflammatory diseases. *Mediators of Inflammation*. 2010. doi:10.1155/2010/802078.

Bancroft, J.D., and C. Layton. 2013. The hematoxylins and eosin. *In* Bancroft's Theory and Practice of Histological Techniques. Elsevier. 173–186.

Betts, J.G., J. Wise, K.A. Young, P. Desaix, E. (Edward W.) Johnson, J.E. Johnson, O. Korol, D. Kruse, B. Poe, M.D. Womble, J.G. Betts, and OpenStax College. 2013. Anatomy and physiology. *In* Anatomy and physiology. 4–25.

Buchwalow, I.B., and W. Böcker. 2010. Immunohistochemistry: Basics and Methods. *Immunohistochemistry: Basics and Methods*. doi:10.1007/978-3-642-04609-4.

Campbell, G.M., and A. Sophocleous. 2014. Quantitative analysis of bone and soft tissue by micro-computed tomography: applications to ex vivo and in vivo studies. *BoneKEy Reports*. 3. doi:10.1038/BONEKEY.2014.59.

D'Elia, G., G. Caracchini, L. Cavalli, and P. Innocenti. 2009. Bone fragility and imaging techniques. *Clinical Cases in Mineral and Bone Metabolism*. 6:234.

Feldman, A.T., and D. Wolfe. 2014. Tissue processing and hematoxylin and eosin staining. *Methods Mol Biol*. 1180:31–43. doi:10.1007/978-1-4939-1050-2_3.

Fischer, A.H., K.A. Jacobson, J. Rose, and R. Zeller. 2008. Hematoxylin and Eosin Staining of Tissue and Cell Sections. *Cold Spring Harbor Protocols*. 2008:pdb.prot4986. doi:10.1101/PDB.PROT4986.

Florencio-Silva, R., G.R. da S. Sasso, E. Sasso-Cerri, M.J. Simões, and P.S. Cerri. 2015. Biology of Bone Tissue: Structure, Function, and Factors That Influence Bone Cells. *BioMed Research International*. 2015:421746. doi:10.1155/2015/421746.

Goodwin, P.C., B. Johnson, and C.W. Frevert. 2018. Microscopy, Immuno-Histochemistry, Digital Imaging, and Quantitative Microscopy. *Comparative Anatomy and Histology*. 53–66. doi:10.1016/B978-0-12-802900-8.00004-X.

Hardouin, P., V. Pansini, and B. Cortet. 2014. Bone marrow fat. *Joint Bone Spine*. 81:313–319. doi:10.1016/j.jbspin.2014.02.013.

Herrmann, M. 2019. Marrow Fat-Secreted Factors as Biomarkers for Osteoporosis. *Current Osteoporosis Reports*. 17:429–437. doi:10.1007/s11914-019-00550-w.

Horge, M., C. Crăciun, S. Tripon, D. Giulei, A. Jompan, A. Hermenean, and C. Roşioru. 2016. MODERATE PHYSICAL ACTIVITY IMPROVES RAT BONE ULTRASTRUCTURE IN

EXPERIMENTAL OSTEOPOROSIS. *Acta Endocrinologica (Bucharest)*. 12:392. doi:10.4183/AEB.2016.392.

Horowitz, M.C., R. Berry, B. Holtrup, Z. Sebo, T. Nelson, J.A. Fretz, D. Lindskog, J.L. Kaplan, G. Ables, M.S. Rodeheffer, and C.J. Rosen. 2017. Bone marrow adipocytes. *Adipocyte*. 6:193–204. doi:10.1080/21623945.2017.1367881.

Idleburg, C., E.N. Delassus, and D. V. Novack. 2015. Immunohistochemistry of skeletal tissues. *Methods in Molecular Biology*. 1226:87–95. doi:10.1007/978-1-4939-1619-1_8.

Johnson, S., and P. Rabinovitch. 2012. Ex vivo imaging of excised tissue using vital dyes and confocal microscopy. *Current Protocols in Cytometry*. CHAPTER:Unit9.39. doi:10.1002/0471142956.cy0939s61.

Kim, T.Y., and A.L. Schafer. 2016a. Diabetes and Bone Marrow Adiposity. *Current Osteoporosis Reports*. 14:337–344. doi:10.1007/s11914-016-0336-x.

Kim, T.Y., and A.L. Schafer. 2016b. Diabetes and Bone Marrow Adiposity. *Curr Osteoporos Rep*. 14:337. doi:10.1007/S11914-016-0336-X.

Longo, A.B., P.L. Salmon, and W.E. Ward. 2017. Comparison of ex vivo and in vivo micro-computed tomography of rat tibia at different scanning settings. *Journal of Orthopaedic Research*. 35:1690–1698. doi:10.1002/jor.23435.

Maity, B., D. Sheff, and R.A. Fisher. 2013. Immunostaining. Detection of Signaling Protein Location in Tissues, Cells and Subcellular Compartments. *In* Methods in Cell Biology. Academic Press Inc. 81–105.

Moen, E., D. Bannon, T. Kudo, W. Graf, M. Covert, and D. van Valen. 2019. Deep learning for cellular image analysis. *Nature Methods 2019 16:12*. 16:1233–1246. doi:10.1038/s41592-019-0403-1.

Nouh, M.R., and A.F. Eid. 2015. Magnetic resonance imaging of the spinal marrow: Basic understanding of the normal marrow pattern and its variant. *World Journal of Radiology*. 7:448. doi:10.4329/wjr.v7.i12.448.

Onul, A., M.D. Colvard, W.A. Paradise, K.M. Elseth, B.J. Vesper, E. Gouvas, Z. Deliu, K.D. Garcia, W.J. Pestle, and J.A. Radosevich. 2012. Application of Immunohistochemical Staining to Detect Antigen Destruction as a Measure of Tissue Damage. *Journal of Histochemistry and Cytochemistry*. 60:683. doi:10.1369/0022155412452146.

Patel, V.S., M.E. Chan, J. Rubin, and C.T. Rubin. 2018. MARROW ADIPOSITY AND HEMATOPOIESIS IN AGING AND OBESITY: EXERCISE AS AN INTERVENTION. *Curr Osteoporos Rep*. 16:105. doi:10.1007/S11914-018-0424-1.

Pham, T.T., K.K. Ivaska, J.C. Hannukainen, K.A. Virtanen, M.E. Lidell, S. Enerbäck, K. Mäkelä, R. Parkkola, S. Piirola, V. Oikonen, P. Nuutila, and R. Kiviranta. 2020. Human Bone Marrow Adipose Tissue is a Metabolically Active and Insulin-Sensitive Distinct Fat Depot. *The Journal of Clinical Endocrinology & Metabolism*. 105:2300–2310. doi:10.1210/CLINEM/DGAA216.

Piotrowska, K., and M. Tarnowski. 2021. Bone Marrow Adipocytes—Role in Physiology and Various Nutritional Conditions in Human and Animal Models. *Nutrients*. 13. doi:10.3390/NU13051412.

Renshaw, S. 2013. Immunohistochemistry and Immunocytochemistry. *In* The Immunoassay Handbook. Elsevier Ltd. 357–377.

Schaffer, D., and S. Willerth. 2017. 5.8 Scaffold materials for human embryonic stem cell culture and differentiation. *In* Comprehensive Biomaterials II. Elsevier. 129–153.

Scheller, E.L., W.P. Cawthorn, A.A. Burr, M.C. Horowitz, and O.A. MacDougald. 2016. Marrow Adipose Tissue: Trimming the Fat. *Trends in Endocrinology & Metabolism*. 27:392–403. doi:10.1016/J.TEM.2016.03.016.

Schindelin, J., I. Arganda-Carreras, E. Frise, V. Kaynig, M. Longair, T. Pietzsch, S. Preibisch, C. Rueden, S. Saalfeld, B. Schmid, J.Y. Tinevez, D.J. White, V. Hartenstein, K. Eliceiri, P. Tomancak, and A. Cardona. 2012. Fiji: an open-source platform for biological-image analysis. *Nature Methods 2012 9:7*. 9:676–682. doi:10.1038/nmeth.2019.

Schnell, S.A., W.A. Staines, and M.W. Wessendorf. 1999. Reduction of lipofuscin-like autofluorescence in fluorescently labeled tissue. *Journal of Histochemistry and Cytochemistry*. 47:719–730. doi:10.1177/002215549904700601.

Shi, S.R., and C.R. Taylor. 2014. Antigen Retrieval in Immunohistochemistry. *Pathobiology of Human Disease: A Dynamic Encyclopedia of Disease Mechanisms*. 3817–3828. doi:10.1016/B978-0-12-386456-7.07404-9.

Styner, M., G.M. Pagnotti, C. McGrath, X. Wu, B. Sen, G. Uzer, Z. Xie, X. Zong, M.A. Styner, C.T. Rubin, and J. Rubin. 2017. Exercise Decreases Marrow Adipose Tissue Through ß-Oxidation in Obese Running Mice. *Journal of Bone and Mineral Research*. 32:1692–1702. doi:10.1002/JBMR.3159.

Tencerova, M., and M. Kassem. 2016. The Bone Marrow-Derived Stromal Cells: Commitment and Regulation of Adipogenesis. *Frontiers in Endocrinology*. 7:127. doi:10.3389/FENDO.2016.00127.

Tratwal, J., R. Labella, N. Bravenboer, G. Kerckhofs, E. Douni, E.L. Scheller, S. Badr, D.C. Karampinos, S. Beck-Cormier, B. Palmisano, A. Poloni, M.J. Moreno-Aliaga, J. Fretz, M.S. Rodeheffer, P. Boroumand, C.J. Rosen, M.C. Horowitz, B.C.J. van der Eerden, A.G. Veldhuis-Vlug, and O. Naveiras. 2020a. Reporting Guidelines, Review of Methodological Standards, and Challenges Toward Harmonization in Bone Marrow Adiposity Research. Report of the Methodologies Working Group of the International Bone Marrow Adiposity Society. *Frontiers in Endocrinology*. 11:1–36. doi:10.3389/fendo.2020.00065.

Wang-Rodriguez, J. 2002. Male Breast Carcinoma: Role of Immunohistochemical Expression of Receptors in Male Breast Carcinoma. *Handbook of Immunohistochemistry and in Situ Hybridization of Human Carcinomas*. 1:477–485. doi:10.1016/S1874-5784(04)80058-8.

Appendix 1

ImageJ script in detail.